THE JOURNAL OF PHYSICAL CHEMISTRY B

Article

pubs.acs.org/JPCB

N-Acylated Dipeptide Tags Enable Precise Measurement of Ion Temperature in Peptide Fragmentation

Jongcheol Seo, Min-Soo Suh, Hye-Joo Yoon, and Seung Koo Shin*

Bio-Nanotechnology Center, Department of Chemistry, Pohang University of Science and Technology, San 31 Hyoja-dong Nam-gu, Pohang, 790-784, Korea

Supporting Information

ABSTRACT: Peptide fragmentations into b- and y-type ions are useful for the identification of proteins. The b ion, having the structure of a N-protonated oxazolone, dissociates to the a-type ion with loss of CO. This CO-loss process affords the possibility of characterizing the temperature of the b ion. Herein, we used N-acylated dipeptide tags, isobaric tags originally developed for protein quantification, as internal standards for the measurement of the ion temperature in peptide fragmentation. Amine-reactive dipeptide tags were attached to the N-termini of sample peptides. Collision-induced dissociation (CID) of the tagged peptides yielded a b-type quantitation signal (b_S) from the tag, which subsequently dissociated into the a_S ion with CO-loss. As the length of alkyl side chain on the dipeptide tag was extended from C_1 to C_8, the yield of a_S ion gradually increased for the 4-alkyl-substituted oxazolone ion but decreased for the 2-alkyl-substituted one. To gain insights into the unimolecular dissociation kinetics, we obtained the potential energy surface from ab initio calculations. Theoretical study suggested that the 4-alkyl substitution on N-protonated oxazolone decreased the enthalpy of activation by stabilizing the productlike transition state, whereas the 2-alkyl substitution increased it by stabilizing the reactant. Resulting potential energy surfaces were used to calculate the microcanonical and canonical rate constants as well as the a_S-ion yield. Arrhenius plots of canonical rate constants provided activation energies and pre-exponential factors for the CO-loss processes in the 600−800 K range. Comparison of experimental a_S-ion yields with theoretical values led to precise determination of the temperature of b_S ion. Thus, the b_S-ion temperature of tagged peptide can be measured simply by combining kinetic parameters provided here and a_S-ion yields obtained experimentally. Although the b-type fragment patterns varied with the chain length and position of alkyl substituent on the N-protonated oxazolone, the y-type fragment patterns were almost identical under these conditions. Furthermore, b_S-ion temperatures were nearly the same with only a few degrees K difference. Our results demonstrate a novel use of N-acylated dipeptide tags as internal temperature standards, which enables the reproducible acquisition of peptide fragment spectra.

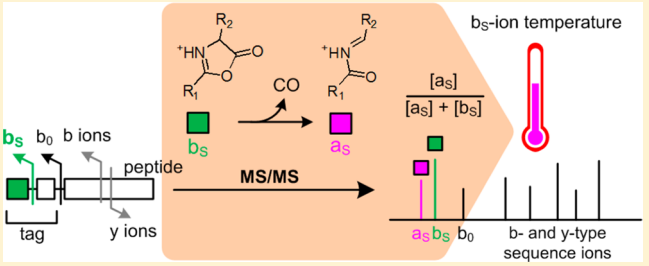

INTRODUCTION

Peptide fragmentations to b-type and complementary y-type ions provide key information about peptide sequence for protein identification.[1−3] Yet the peptide fragment spectra are usually different from laboratory to laboratory and even from one period of experiment to another in the same laboratory. Because there is no standard for obtaining peptide fragment spectra, the mass spectral database for peptide fragmentation is not comparable among laboratories. When electron ionization (EI) was the most important ionization method, the standard mass spectra of small molecules were obtained by applying a kinetic energy of 70 eV.[4] This electron kinetic energy was sufficiently high to ionize any molecule and also to cause fragmentation, which provided information about molecular structure. In the cases of matrix-assisted laser desorption ionization (MALDI)[5] and electrospray ionization (ESI),[6] which are the two most widely used ionization methods for characterizing peptides and biomolecules, there have been no standard protocols for measuring the mass spectra because of highly specialized and generally proprietary nature of ionization methods and also because of the difficulty in controlling the temperature or internal energy of ionized molecules. Unlike EI, both MALDI and ESI are designed to yield the peptide molecular ion without severe fragmentation; thus, peptide fragmentation is separately induced by collision in tandem mass spectrometry (MS/MS). If we can measure the temperature of collisionally activated peptide ions, it might be possible to obtain the peptide fragment spectra reproducibly at similar ion temperatures. Besides, peptide/fragment ion temperatures can provide valuable information about thermochemical kinetics of peptide fragmentation and structural changes in peptide ions. To this end, we need to develop a robust tool that is applicable to both MALDI and ESI-MS/MS techniques.

Received: September 1, 2012
Revised: November 6, 2012
Published: November 8, 2012

dx.doi.org/10.1021/jp308697v | J. Phys. Chem. B 2012, 116, 13982−13990

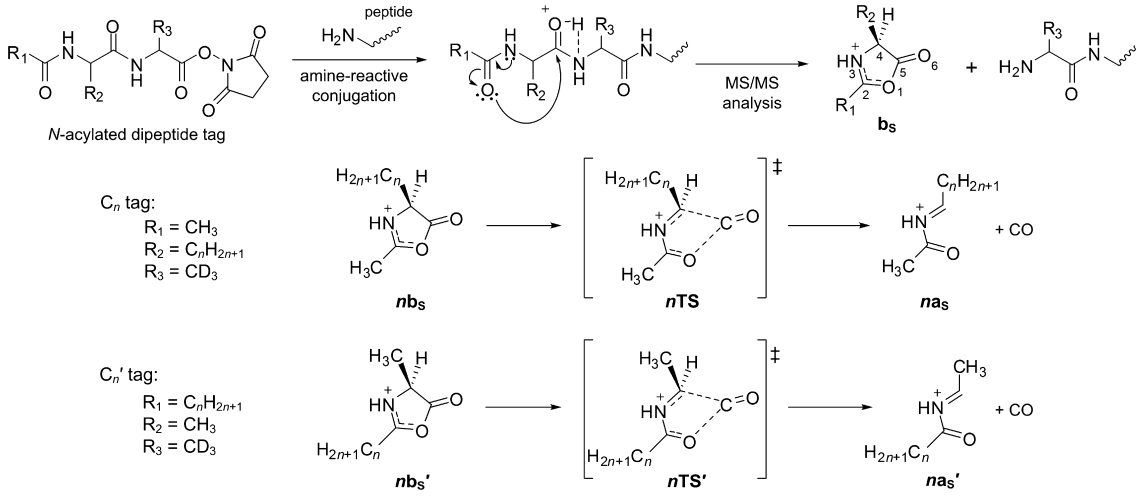

Figure 1. N-Acylated dipeptide tags (C_n and C_n' tags; n = 1−8), amine-reactive conjugation to the peptide, and production of the N-protonated oxazolone ion (b_S) upon MS/MS analysis. ***n*b$_S$** (N-protonated 2-methyl-4-alkyloxazol-5-one) and ***n*b$_S$′** (N-protonated 2-alkyl-4-methyloxazol-5-one) ions originated from C_n and C_n' tags dissociate to ***n*a$_S$** and ***n*a$_S$′** ions with loss of CO via transition states ***n*TS** and ***n*TS′**, respectively.

To date, only a few studies have reported the measurement of the "effective" temperature of peptide ions,[7−12] although several "thermometer" ions have been suggested for the estimation of the extent of internal excitation and the temperature of small molecular ions.[13−15] Tomer and co-workers as well as Glish and co-workers measured the ratio of the most prominent fragment ions derived from leucine enkephalin ions to determine the amount of internal energy deposited by collision.[7,8] Williams and co-workers obtained kinetic parameters for blackbody infrared radiative dissociation of bradykinin and its analogues[9] as well as leucine enkephalin[10] in the ion cyclotron resonance (ICR) cell and applied those kinetic parameters to the estimation of temperatures of leucine enkephalin and bradykinin ions.[11] Kim and co-workers obtained kinetic parameters for postsource decay and photodissociation of small peptide ions generated by MALDI and determined the effective ion temperature by modeling survival yields.[12] The key for temperature measurement was kinetic parameters, such as the energy of activation E_a and the entropy of activation $\Delta S^{\ddagger}$. However, these kinetic parameters significantly vary with the peptide sequence and the charge state.[11,12] Thus, this approach, based on unimolecular dissociation of the whole peptide ion, requires separate kinetic parameters for each charge state of every peptide prior to determination of the ion temperature. To circumvent this problem, we developed an internal standard method that could be applied to measure the peptide ion temperature. N-Acylated dipeptide tags were attached to the N-termini of peptides as internal standards, and the unimolecular dissociation kinetics of the b-type N-protonated oxazolone ion derived from the tag was used to measure the ion temperature.

N-Acylated dipeptide tags have been introduced by our group as the mass-balanced H/D-isotope-coded dipeptide tag (MBIT) for simultaneous identification and quantification of peptides.[16−18] They are composed of an *N*-acyl group with an alkyl moiety R_1, an aliphatic amino acid with an alkyl side chain R_2, an alanine having a methyl group R_3, and an *O*-succinimidyl ester (OSu), as shown in Figure 1. The amine-reactive OSu linker is used for the conjugation of tags to the N-termini of sample peptides. A linear alkyl chain (C_nH_{2n+1}, n = 1−8) is placed either at R_2 of the aliphatic amino acid for the C_n tag or at R_1 of the *N*-acyl group for the C_n' tag. A methyl group is placed at R_1 for the C_n tag and at R_2 for the C_n' tag. Thus, upon MS/MS analysis of the peptide ion, the C_n tag results in N-protonated 2-methyl-4-alkyloxazol-5-one (***n*b$_S$**), whereas the C_n' tag yields N-protonated 2-alkyl-4-methyloxazol-5-one (***n*b$_S$′**). ***n*b$_S$** and ***n*b$_S$′** ions subsequently dissociate to ***n*a$_S$** and ***n*a$_S$′** ions with CO-loss via ***n*TS** and ***n*TS′** transition states, respectively. An isobaric pair of 2-plex quantitation tags can be made by placing CH_3 and CD_3 alternately at R_1 and R_3 for C_n tags and at R_2 and R_3 for C_n' tags. A series of 2-plex C_n tags has been successfully used in multi 2-plex quantification of proteins.[17]

The structure of the b_S ion is considered to be N-protonated oxazolone,[19−24] which undergoes CO-loss to yield the a_S ion. The mechanism and energetics of this CO-loss process have been studied extensively because both a- and b-type ions are frequently detected in the spectra. Theoretical studies have suggested that the transition state involves cleavage of both O(1)−C(5) and C(4)−C(5) bonds to release C(5)O(6) and the resulting a_S ion has the structure of protonated imine.[25−27] Paizs et al. have examined the effects of isobutyl substitution at C(2) and C(4) on the transition state and found that the 4-butyl substitution lowers the activation barrier by stabilizing the transition state more than the 2-butyl substitution does.[25] Therefore, the activation energy for the CO-loss process can be controlled by placing an alkyl group at C(2) and C(4), as shown in Figure 1. Moreover, the effects of an alkyl substituent on the kinetics of unimolecular dissociation of the b_S ion can be examined by measuring the a_S-ion yield.

In this work, both C_n and C_n' tags (n = 1−8) were conjugated to the two sample peptides, [Glu^1]-fibrinopeptide B and bradykinin. Singly and doubly protonated peptide ions labeled with C_n or C_n' tags were produced by MALDI and ESI, respectively. Mass-selected peptide ions were then dissociated into b_S ions (***n*b$_S$** and ***n*b$_S$′**) by MS/MS. Yields of a_S ions (***n*a$_S$** and ***n*a$_S$′**) were obtained from the MS/MS spectra as a function of alkyl chain length n = 1 to 8. To gain insights into the potential energy surface of the unimolecular dissociation reaction, we determined the geometries, energies, and vibrational frequencies of b_S ions, transition states, and a_S ions from ab initio calculations. On the basis of the ab initio potential energy surface, we first obtained the microcanonical rate constant using the Rice−Ramsperger−Kassel−Marcus

dx.doi.org/10.1021/jp308697v | J. Phys. Chem. B 2012, 116, 13982−13990

(RRKM) theory[28] and then calculated the canonical rate constant by integrating the microcanonical rate constant over the internal energy distribution of the b_S ion. The a_S-ion yield obtained experimentally was compared with the theoretical yield to determine the b_S-ion temperature. Results showed that the a_S-ion yield served as a precise measure of the b_S-ion temperature in both MALDI- and ESI-MS/MS. Furthermore, the y-type fragment spectra were reproducible when the b_S-ion temperatures were nearly the same.

MATERIALS AND METHODS

Materials. $C_1'-C_8'$ and C_1-C_5 tags were prepared in the laboratory by the solid-phase synthesis[16−18] and C_6-C_8 tags were synthesized by olefin metathesis reactions in solution, as previously described in detail.[17] [Glu[1]]-fibrinopeptide B (EGVNDNEEGFFSAR) and bradykinin (RPPGFSPFR) were purchased from Sigma−Aldrich (St. Louis, MO). Acetonitrile (ACN, HPLC-grade), dimethylformamide (DMF, anhydrous), trifluoroacetic acid (TFA, HPLC-grade), hydroxylamine hydrochloride, and 4-hydroxy-α-cyanocinnamic acid (HCCA) were obtained from Sigma−Aldrich.

Conjugation of N-Acylated Dipeptide Tags to Peptides. Either C_n or C_n' tags were conjugated to sample peptides by mixing peptides (0.4 mM in 100 mM sodium bicarbonate buffer) with a solution containing C_n or C_n' tags (35 mM in DMF) in a 1:1 (v/v) ratio, as previously described.[17] After incubation of the reaction mixture for more than 6 h at room temperature, hydroxylamine hydrochloride (80 mM in 100 mM sodium bicarbonate buffer) was added and the reaction mixture was stirred for another 6 h to reverse side reactions at tyrosine, threonine, and serine, as well as to consume excess C_n or C_n' tags.[16] The conjugation reaction was terminated by addition of 10% TFA.

MALDI and ESI Mass Spectrometry. For MALDI-MS, peptides labeled with C_n or C_n' tags were diluted in a 1:1 ACN/H_2O solution containing 1% TFA (v/v) (50TA) to a final concentration of 0.5 μM. The peptide solution was mixed with matrix (5 mg of HCCA in 1 mL of 50TA) in a 1:1 (v/v) ratio and loaded on a MALDI plate (250 fmol per spot). The MALDI mass spectra of singly protonated peptides were acquired by taking an average of 2000 laser shots using a MALDI time-of-flight (TOF) mass spectrometer (4700 Proteomics Analyzer, AB Sciex, Foster City, CA). For the MALDI-TOF/TOF MS/MS analysis, the precursor ion was accelerated to a kinetic energy of approximately 1 keV before entering a collision cell containing air (1.3×10^{-6} Torr). For ESI-MS, peptides labeled with C_n or C_n' tags were diluted in a 1:1 ACN/H_2O solution containing 1% formic acid (v/v) to a final concentration of 0.5 μM. The peptide solution (5 μL) was loaded on a 1-μm i.d. Au/Pd-coated borosilicate emitter (Proxeon, Odense, Denmark) and electrosprayed into a hybrid triple quadrupole TOF mass spectrometer (Q-TOF Premiere, Waters, Manchester, UK). The voltage on the nanospray emitter was 1.8 kV. The ESI-Q-TOF MS/MS spectra of doubly protonated peptides were acquired by accelerating ions with a bias voltage of 30 V for bradykinin and of 40 V for [Glu[1]]-fibrinopeptide B. Argon (2.4×10^{-3} Torr) was used as a collision gas. Each mass spectrum was obtained from an average of 60 0.5-s scans.

Theoretical Calculations. Geometries, total energies, and vibrational frequencies of the b_S and a_S ions as well as the transition states were calculated at the Becke three-parameter Lee−Yang−Parr (B3LYP) level of density functional theory (DFT) with a 6-31++G(d,p) basis set using a Gaussian03 program.[29] All calculations were performed for hydrogenated species only. The structure of b_S ion was optimized as the N-protonated oxazolone ion. The a_S ion was optimized after removing CO from the b_S ion. The transition state was searched between the optimized b_S and a_S geometries using a synchronous transit-guided quasi-Newton method.[30] Vibrational frequencies were scaled by a factor of 0.9806 and zero-point energy (ZPE) was calculated from the scaled frequencies.[31] The total energy was corrected for ZPE, and the entropy was calculated from the vibrational partition function.

The microcanonical rate constant $k(E)$ for unimolecular dissociation of the b_S ion was calculated as a function of internal energy E using the RRKM theory, as expressed in eq 1,[28]

$$k(E) = \frac{W^{\ddagger}(E - E_0 - E_r^{\ddagger})}{h\rho(E - E_r)} \tag{1}$$

where $W^{\ddagger}(E - E_0 - E_r^{\ddagger})$ is the sum of vibrational states of the transition state (***n*TS** or ***n*TS′**), $\rho(E - E_r)$ is the density of vibrational states of the b_S ion (***n*b$_S$** or ***n*b$_S$′**), and h is the Planck's constant. E is the internal energy of the b_S ion and E_0 is the energy of activation at 0 K for the transition state relative to the b_S ion. E_r and $E_r^{\ddagger}$ are the rotational energies of the b_S ion and the transition state, respectively. The sum and density of states were calculated using a Beyer−Swinehart direct counting algorithm[28] with 1 cm^{-1} bin size. Internal rotations and all vibrational modes were treated as harmonic oscillators. External rotations were treated as adiabatic rotors, thus subtracting the rotational energy (E_r or $E_r^{\ddagger}$) from the internal energy E in state counting. The canonical rate constant $k(T)$ was calculated by integrating $k(E)$ over the thermal internal energy distribution $P(E)$ of the b_S ion, as expressed in eqs 2−4,[28]

$$k(T) = \int_0^{\infty} k(E)P(E)\mathrm{d}E \tag{2}$$

$$P(E) = \frac{\rho(E)\exp(-E/k_BT)}{Q} \tag{3}$$

$$Q = \sum_{E=0}^{\infty} \rho(E)\exp(-E/k_BT) \tag{4}$$

where $\rho(E)$ and Q are the density of vibrational states and the vibrational partition function of the b_S ion, respectively, and k_B is the Boltzmann constant. The temperature of the b_S ion was varied from 600 to 800 K for $k(E)$ and $k(T)$ calculations.

In addition, the yield of a_S ion was obtained by calculating the probability of the a_S-ion formation from unimolecular dissociation of the b_S ion during the transit of the tagged peptide ion through a collision cell. The a_S-ion yield, the ratio of relative abundance of the a_S ion to that of the sum of a_S and b_S ions, was obtained from $k(T)$ using eq 5.

$$\frac{[a_S]}{([a_S] + [b_S])} = \frac{1}{\tau}\int_0^{\tau}(1 - e^{-k(T)t})\mathrm{d}t = 1 - \frac{1 - e^{-k(T)\tau}}{k(T)\tau} \tag{5}$$

where τ is the transit time of the tagged peptide ion traversing a collision cell. τ was determined from the kinetic energy (E_{tr}) of the peptide ion and path length (L) in the collision cell using eq 6.

dx.doi.org/10.1021/jp308697v | J. Phys. Chem. B 2012, 116, 13982−13990

$$\tau = \frac{L}{\sqrt{2E_{tr}/m}} \quad (6)$$

where m is the mass of the peptide ion. E_{tr} was 1 keV for singly charged ions in MALDI-TOF/TOF or 60 and 80 eV for doubly charged bradykinin and [Glu^1]-fibrinopeptide B in ESI-Q-TOF, respectively. L was 10 and 18.5 cm in MALDI-TOF/TOF and ESI-Q-TOF, respectively. τ was approximately 7 μs in TOF/TOF and 60 μs in Q-TOF for C_n or C_n' tag-labeled bradykinin, and 8 μs in TOF/TOF and 72 μs in Q-TOF for C_n or C_n' tag-labeled [Glu^1]-fibrinopeptide B.

RESULTS

MS/MS of MBIT-Linked Peptides. Low-mass region of the MS/MS spectra is shown in Figure 2 for both singly and doubly protonated [Glu^1]-fibrinopeptide B labeled with C_n or C_n' tags (n = 2, 5, and 8), as an example. The full-scale mass spectra are displayed in Figures S1−S4 in the Supporting Information.

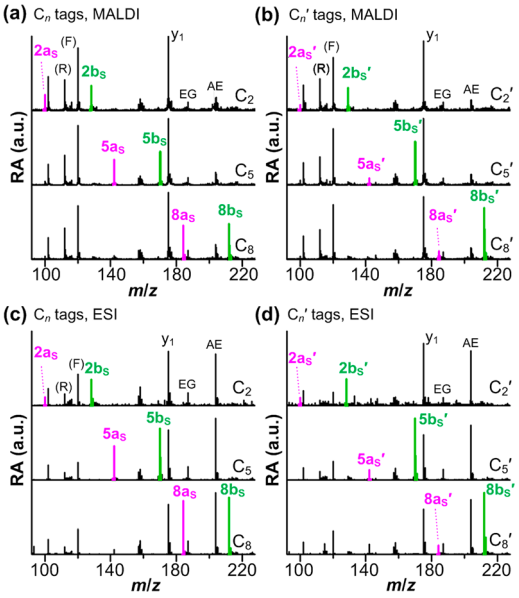

Figure 2. Low-mass region (m/z 80−230) of the MALDI-MS/MS spectra of singly protonated [Glu^1]-fibrinopeptide B labeled with (a) C_n and (b) C_n' tags and that of the ESI-MS/MS spectra of doubly protonated [Glu^1]-fibrinopeptide B labeled with (c) C_n and (d) C_n' tags. a_S and b_S ions are colored in magenta and green, respectively. Immonium ions are shown in parentheses. EG and AE denote internal fragment ions. RA, relative abundance in arbitrary units (au).

All of the a_S and b_S ions were singly charged, regardless of the charge state of the tagged peptide ions. The b_S ion appeared at m/z 128.1 from both C_2 and C_2' tags, 170.2 from both C_5 and C_5' tags, and 212.2 from both C_8 and C_8' tags, showing an m/z increment of 42 (three CH_2 units). a_S ions at m/z 100.1, 142.1, and 184.1 also showed an increment of 42. Notably, some peaks, such as the y_1 ion, immonium ions, and internal fragment ions, appeared at fixed m/z values, independent of the C_n and C_n' tags. As the alkyl chain length was extended in both C_n and C_n' tags, the relative abundance of a_S + b_S increased independently of the charge state of the precursor ions (data not shown). However, the a_S-ion yield, $[a_S]/([a_S] + [b_S])$, showed a remarkable difference between C_n and C_n' tags, as depicted in Figure 3. In the case of singly protonated [Glu^1]-fibrinopeptide B, the a_S-ion yield increased from 0.37 with the

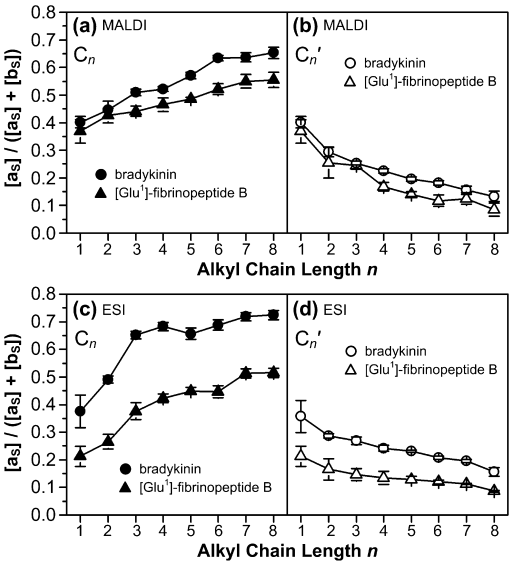

Figure 3. Yield of the a_S ion relative to the abundance of a_S + b_S from the MALDI-MS/MS spectra of singly protonated bradykinin and [Glu^1]-fibrinopeptide B labeled with (a) C_n and (b) C_n' tags, and the a_S-ion yield from the ESI-MS/MS spectra of doubly protonated bradykinin and [Glu^1]-fibrinopeptide B labeled with (c) C_n and (d) C_n' tags.

C_1 tag to 0.53 with the C_8 tag (Figure 3a) but decreased from 0.37 with the C_1' tag to 0.09 with the C_8' tag (Figure 3b). Note that the C_1' tag is identical to the C_1 tag. Analogous results were obtained with singly protonated bradykinin. With doubly protonated ions, both peptides showed a similar trend of a_S-ion yields to singly protonated peptides (an increase with C_n tags and a decrease with C_n' tags) as the alkyl chain length of the tags increased (Figure 3c,d). Because C_n and C_n' tags resulted in protonated oxazolone ions with 4- and 2-alkyl substitutents, respectively, our results suggest that the position of the alkyl substituent on the protonated oxazolone ion modulates the kinetics of the CO-loss process.

Optimized Molecular Structures. Of the b_S ions, the propyl-substituted ones derived from C_3 and C_3' tags are presented in Figure 4. Optimized geometries of **3b$_S$**, **3b$_S$′**, **3TS**, **3TS′**, **3a$_S$**, and **3a$_S$′** as well as ZPE-corrected total energies (in hartrees) are shown. Total energies and ZPEs for all other ions are summarized in Table S1 in the Supporting Information. For both **3b$_S$** and **3b$_S$′**, the proton was localized at N(3) and the oxazolone ring was planar. Importantly, the 2-alkyl substituent was in plane with the ring, whereas the 4-alkyl substituent was out of plane from the ring. The bond lengths of 1.32 Å for O(1)−C(2) and 1.31 Å for C(2)−N(3) suggest a significant double bond character for both bonds. The C−C bond length of 1.48 Å between C(2) and the in-plane 2-alkyl substituent R_1 in **3b$_S$′** was somewhat shorter than that of 1.54 Å between C(4) and the out-of-plane 4-alkyl substituent R_2 in **3b$_S$**. This difference in bond length indicates that the in-plane 2-alkyl substituent interacts with the ring more strongly than the out-of-plane 4-alkyl substituent, thereby stabilizing the b_S ion better. In fact, the total energy suggests that **3b$_S$′** is 0.65 kcal mol^{-1} more stable than **3b$_S$**. The structures of transition states (**3TS** and **3TS′**) were productlike with C(5)O(6) asymmetrically detached from the oxazolone ring. In the cases of **3a$_S$** and **3a$_S$′** with the proton localized at N(3), the O(1)−C(2) bond was contracted to 1.19 Å, thus becoming a carbonyl double bond, whereas the C(2)−N(3) bond was extended to a single bond of

dx.doi.org/10.1021/jp308697v | J. Phys. Chem. B 2012, 116, 13982−13990

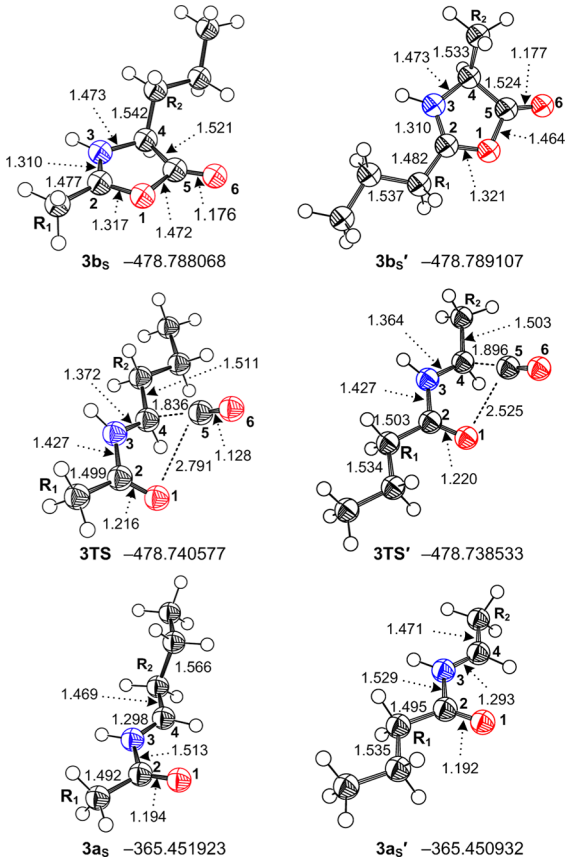

Figure 4. Optimized geometries at the B3LYP/6-31++G(d,p) level for the b_S ion (**3b**$_S$ and **3b**$_S$′), the transition state (**3TS** and **3TS**′), and the a_S ion (**3a**$_S$ and **3a**$_S$′) derived from C_3 and C_3′ tags. Carbon is colored in black, nitrogen in blue, and oxygen in red. Open circle denotes hydrogen. ZPE-corrected total energy is given in hartrees and distance in angstroms.

1.51−1.53 Å. Meanwhile, the N(3)−C(4) bond length was reduced to 1.29−1.30 Å with a significant double bond character. The C−C bond length of 1.47 Å between C(4) and the 4-alkyl substituent R_2 in **3a**$_S$ was slightly shorter than that of 1.50 Å between C(2) and the 2-alkyl substituent R_1 in **3a**$_S$′, indicating that the 4-alkyl substituent stabilizes the a_S ion better than the 2-alkyl substituent. Because the transition state is productlike, the 4-alkyl substituent also stabilizes the transition state better than the 2-alkyl substituent.

Enthaply of Reaction and Enthalpy of Activation. Differences in ZPE-corrected total energy E between ***n*b**$_S$ and ***n*b**$_S$′ [$\Delta E(\mathbf{b_S}) = E(n\mathbf{b_S}') - E(n\mathbf{b_S})$], between ***n*a**$_S$ and ***n*a**$_S$′ [$\Delta E(\mathbf{a_S}) = E(n\mathbf{a_S}') - E(n\mathbf{a_S})$], and between ***n*TS** and ***n*TS**′ [$\Delta E(\mathbf{TS}) = E(n\mathbf{TS}') - E(n\mathbf{TS})$] are shown in Figure 5a as a function of alkyl chain length. As the alkyl chain length increased, $\Delta E(\mathbf{b_S})$ slowly decreased, whereas both $\Delta E(\mathbf{a_S})$ and $\Delta E(\mathbf{TS})$ gradually increased. The 2-alkyl substituent lowered the energy level of the b_S ion, whereas the 4-alkyl substituent stabilized the a_S ion as well as the transition state. Thus, the 2-alkyl substitution increased the enthalpy of activation at 0 K, $\Delta H^{\ddagger}_{0K}$ (= E(TS) − $E(b_S)$), whereas the 4-alkyl substitution decreased it. At 0 K, $\Delta H^{\ddagger}_{0K}$ is equal to E_0, the energy of activation. $\Delta H^{\ddagger}_{0K}$ is plotted in Figure 5b as a function of enthalpy of reaction at 0 K, ΔH_{0K} (= $E(a_S) - E(b_S)$), for n = 1−8. Consequently, the 2-alkyl substituent increased both $\Delta H^{\ddagger}_{0K}$ and ΔH_{0K}, whereas the 4-alkyl substituent decreased

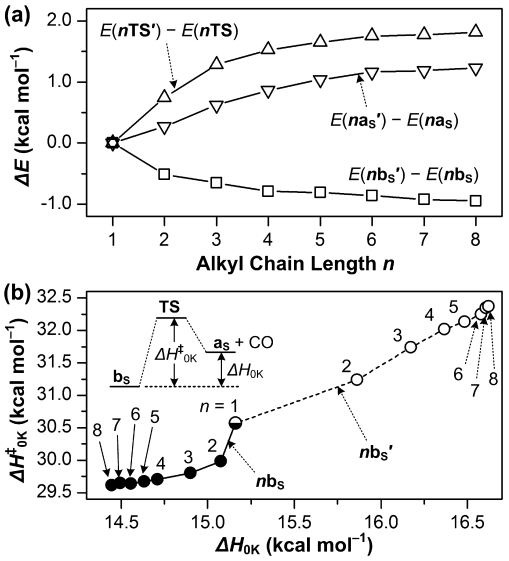

Figure 5. (a) Difference in ZPE-corrected energy E as a function of the alkyl chain length n. (b) Enthalpy of activation at 0 K ($\Delta H^{\ddagger}_{0K}$) vs enthalpy of reaction at 0 K (ΔH_{0K}) for the unimolecular dissociation of b_S to a_S with loss of CO via the transition state TS. **1b**$_S$ and **1a**$_S$ are identical to **1b**$_S$′ and **1a**$_S$′, respectively.

both. Note that **1b**$_S$ and **1b**$_S$′ are the same protonated 2,4-dimethyloxazol-5-one with $\Delta H^{\ddagger}_{0K}$ of 30.6 kcal mol^{-1} and ΔH_{0K} of 15.2 kcal mol^{-1}. As the alkyl chain length increased from 2 to 8, $\Delta H^{\ddagger}_{0K}$ and ΔH_{0K} for ***n*b**$_S$′ increased linearly from 31.2 to 32.4 kcal mol^{-1} and from 15.9 to 16.6 kcal mol^{-1}, respectively. In contrast, $\Delta H^{\ddagger}_{0K}$ and ΔH_{0K} for ***n*b**$_S$ decreased linearly from 30.0 to 29.6 kcal mol^{-1} and from 15.1 to 14.4 kcal mol^{-1}, respectively. Notably, for ***n*b**$_S$ the activation enthalpy ($\Delta H^{\ddagger}_{0K}$) remained nearly the same with n = 6−8, whereas for ***n*b**$_S$′ the reaction enthalpy (ΔH_{0K}) remained almost constant with n = 6−8.

Kinetics of Unimolecular Dissociation, Arrhenius Activation Parameters, and Ion Temperature. The enthalpy of activation, vibrational frequencies, and rotational constants were used to calculate the microcanonical rate constant $k(E)$ for the unimolecular dissociation of the b_S ion. As an example, values of $k(E)$ obtained at 700 K (temperature assigned to adiabatic rotors) for the alkyl chain length n = 1, 2, 4, and 8 are plotted as a function of internal energy E in Figure 6a. The internal energy distribution $P(E)$ for ***n*b**$_S$ and ***n*b**$_S$′ at 700 K is also compared in Figure 6b. Each pair of ***n*b**$_S$ and ***n*b**$_S$′ exhibited an identical internal energy distribution. As the alkyl chain length increased, the average internal energy increased significantly; however, the rate constant $k(E)$ decreased gradually because the density of states for ***n*b**$_S$ or ***n*b**$_S$′ increased with increasing internal degrees of freedom. The difference in $k(E)$ between ***n*b**$_S$ and ***n*b**$_S$′ became larger with increasing alkyl chain length because the difference in $\Delta H^{\ddagger}_{0K}$ between the two isobaric b_S ions increased. The microcanonical rate constant $k(E)$ was converted to the canonical rate constant $k(T)$ in the temperature range of 600−800 K using eqs 2−4 (see Materials and Methods). The logarithm of $k(T)$ for ***n*b**$_S$ and ***n*b**$_S$′ (n = 1, 2, 4, and 8) is displayed as a function of the inverse of temperature in Figure 6c. As the alkyl chain length increased, $k(T)$ for ***n*b**$_S$ increased, whereas $k(T)$ for ***n*b**$_S$′ decreased. Arrhenius plots (Figure 6c) of $k(T)$ for ***n*b**$_S$ yielded the activation energy (E_a) of 31.5−32.4 kcal mol^{-1} from the slope and the pre-exponential factor (A) of (1.4−1.9) × 10^{15} s^{-1} from

dx.doi.org/10.1021/jp308697v | J. Phys. Chem. B 2012, 116, 13982−13990

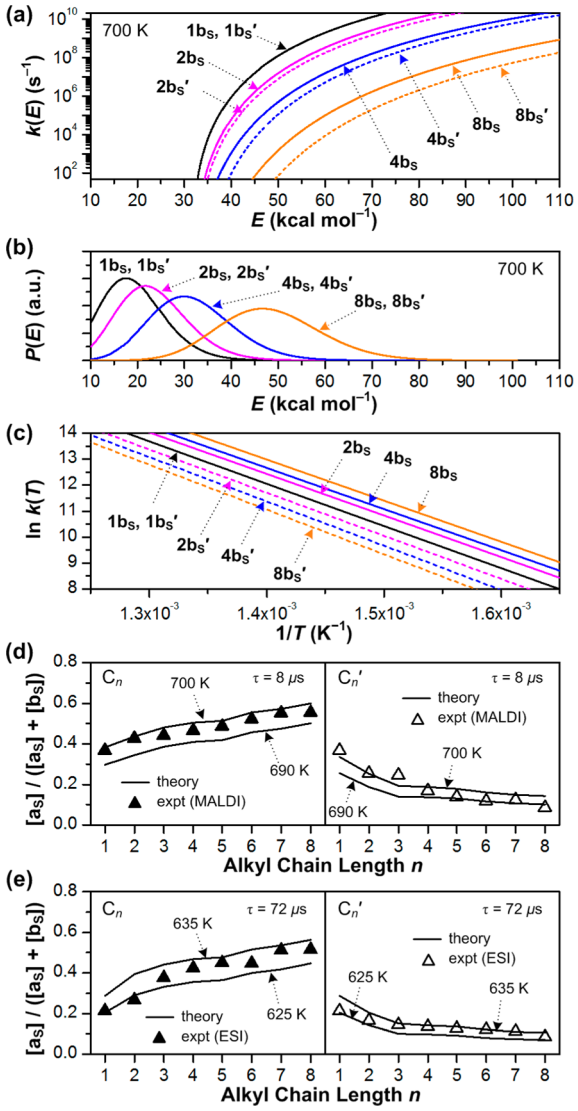

Figure 6. (a) Microcanonical rate constant $k(E)$ for reactions $n\mathbf{b}_S \rightarrow n\mathbf{a}_S + CO$ and $n\mathbf{b}_S' \rightarrow n\mathbf{a}_S' + CO$ (n = 1, 2, 4, and 8) as a function of internal energy E. The temperature of the adiabatic rotor was set at 700 K. (b) Internal energy distribution $P(E)$ of $n\mathbf{b}_S$ and $n\mathbf{b}_S'$ at 700 K in arbitrary units (au). $P(E)$ for $n\mathbf{b}_S'$ (hidden) overlaps with $P(E)$ for $n\mathbf{b}_S$ (solid line). (c) Arrhenius plot of the canonical rate constant $k(T)$ as a function of T^{-1}. (d, e) The a_S-ion yield obtained from [Glu^1]-fibrinopeptide B labeled with C_n and C_n' tags using MALDI-TOF/TOF for singly protonated peptides (d) and ESI-Q-TOF for doubly protonated peptides (e); experiments (triangle) and theory (line). τ is the transit time of the peptide ion in a collision cell.

the intercept. In the case of $n\mathbf{b}_S'$, E_a was 32.4−34.2 kcal mol^{-1} and A was (1.5−2.1) × 10^{15} s^{-1}. Arrhenius parameters (E_a and A) for the b_S ion derived from all of the C_n and C_n' tags are listed in Table 1. Using these parameters, $k(T)$ can be evaluated in the temperature range of 600−800 K conversely from the Arrhenius equation, $k(T) = A \exp(-E_a/RT)$, where R is the gas constant.

To determine the b_S-ion temperature, we compared the a_S-ion yield, $[a_S]/([a_S] + [b_S])$, obtained from experiments with the theoretical yield calculated from $k(T)$ and the transit time τ using eq 5 (see Materials and Methods). Results from singly and doubly protonated [Glu^1]-fibrinopeptide B are displayed in Figure 6d and e, respectively. Yields of a_S ions from experiments

Table 1. Arrhenius Parameters, Activation Energy (E_a), and Pre-exponential Factor (A) in the Temperature Range of 600−800 K

	$n\mathbf{b}_S \rightarrow n\mathbf{a}_S$ from C_n tags		$n\mathbf{b}_S' \rightarrow n\mathbf{a}_S'$ from C_n' tags	
n	E_a (kcal mol^{-1})	A (10^{15} s^{-1})	E_a (kcal mol^{-1})	A (10^{15} s^{-1})
1	32.4	1.5	32.4	1.5
2	31.9	1.4	33.1	1.6
3	31.6	1.6	33.5	1.7
4	31.6	1.5	33.9	1.8
5	31.5	1.5	34.0	2.1
6	31.5	1.7	34.1	2.0
7	31.5	1.8	34.2	1.9
8	31.5	1.9	34.2	1.9

were bracketed by theoretical yields calculated at 690 K and at 700 K in Figure 6d for singly protonated fibrinopeptides labeled with C_n or C_n' tags. Thus, the b_S-ion temperature was assigned as 695 ± 5 K. Meanwhile, the b_S-ion temperature was bracketed between 625 K and 635 K for doubly protonated fibrinopeptides labeled with C_n or C_n' tags (Figure 6e). The b_S-ion temperature obtained from MALDI-TOF/TOF was on average 65 ± 5 K higher than that from ESI-Q-TOF. Apparently, the b_S ion that underwent unimolecular dissociation within 8 μs of the transit time in TOF/TOF had an internal energy much higher than the b_S ion that lost CO within 72 μs in Q-TOF. Nonetheless, for each MS/MS setup, the b_S-ion temperatures were determined to be almost identical to each other within ±5 K, independent of the alkyl chain length of the tag. With another peptide bradykinin, the b_S-ion temperature was bracketed in the range of 708−718 K for singly protonated peptides produced in MALDI-TOF/TOF and of 650−658 K for doubly protonated peptides generated in ESI-Q-TOF (see Tables S2 and S3 in the Supporting Information). Again, the difference in b_S-ion temperatures was within ±5 K for each MS/MS setup. Thus, the b_S-ion temperature of tagged peptides can be determined by combining kinetic parameters provided in Table 1 and experimental a_S-ion yields using both MALDI-TOF/TOF and ESI-Q-TOF MS/MS techniques. Interestingly, as the transit time τ of the precursor ion in a collision cell increased from 7 μs for singly protonated bradykinin to 8 μs for singly protonated fibrinopeptide and from 60 μs for doubly protonated bradykinin to 72 μs for doubly protonated fibrinopeptide, the b_S-ion temperature decreased from 713 ± 5 K to 695 ± 5 K and from 654 ± 4 K to 630 ± 5 K, respectively. This result indicates that the shorter the transit time, the higher the required internal energy.

Peptide Fragmentation Pattern. Because the b_S-ion temperatures from all C_n and C_n' tags were nearly identical at a fixed transit time, we examined the peptide fragment spectra to see if the fragmentation patterns were comparable to each other. Relative abundances of y- and a/b-type ions were extracted from the peptide mass spectra (see Figures S1−S4) of [Glu^1]-fibrinopeptide B labeled with C_n or C_n' tags (n = 2, 5, 8), as shown in Figure 7. Results from bradykinin are presented in Figure S5 in the Supporting Information. While most of the b ions were confined in a low-mass region, y ions were distributed in a wide mass range, constituting most of the peptide fragment spectra for sequencing. None of the y ions carried C_n or C_n' tag at their N-termini, and their relative abundances were almost identical for both fibrinopeptide (Figure 7a,d) and bradykinin (Figure S5a,d). Only a small, sequence-related variation was observed. On the other hand, all

dx.doi.org/10.1021/jp308697v | J. Phys. Chem. B 2012, 116, 13982−13990

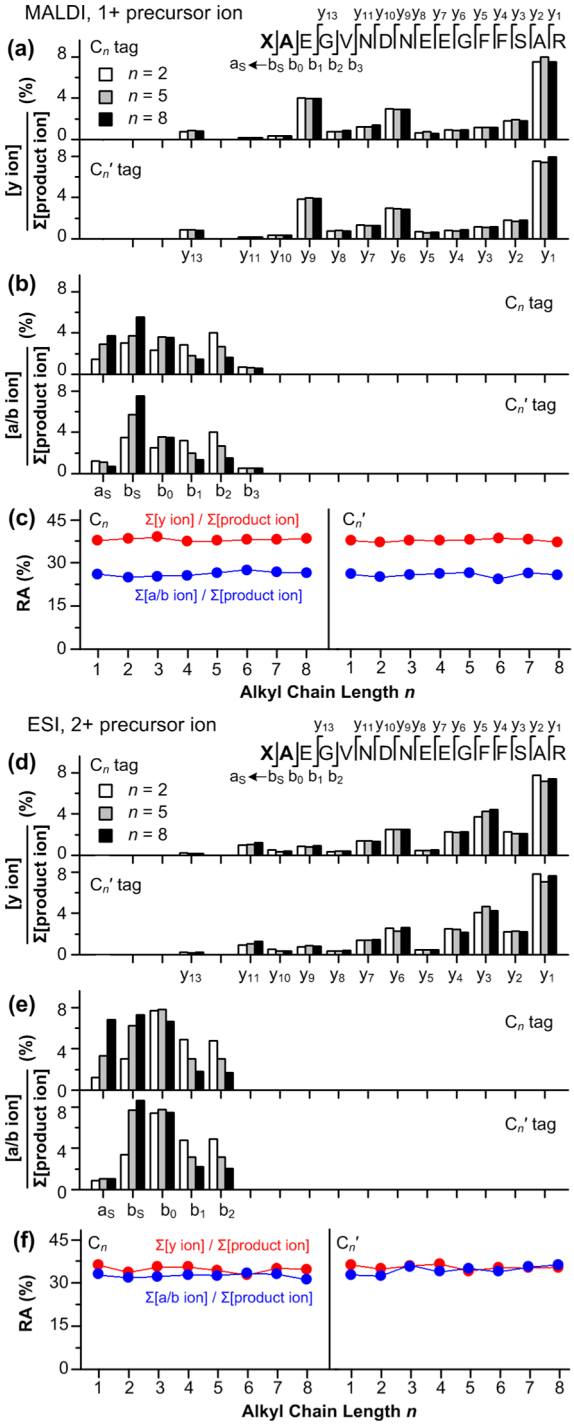

Figure 7. Relative abundances of (a) y-type fragment ions, (b) a/b-type fragment ions, and (c) the sum of all y and a/b ions with respect to total product ions obtained from singly protonated [Glu[1]]-fibrinopeptide B labeled with C_n or C_n' tag. Relative abundances of (d) y ions, (e) a/b ions, and (f) the sum of all y and a/b ions from doubly protonated C_n or C_n'-tagged [Glu[1]]-fibrinopeptide B. X represents the N-acylated amino acid in the tag. n = 2, 5, and 8 in parts a, b, d, and e; n = 1−8 in parts c and f.

of the b ions excluding b_S contained the tag, and their relative abundances exhibited a significant variation with alkyl chain length (Figure 7b,e; Figure S5b,e). Nevertheless, the sum of relative abundances of all y and a/b ions relative to total fragment ions remained almost constant, regardless of the alkyl chain length, as shown in Figure 7c,f (see Figure S5c,f for bradykinin). As the charge state increased from 1+ to 2+, the sum of relative abundances of a/b ions from fibrinopeptide increased, whereas that from bradykinin decreased. Although peptide fragmentation patterns depended on the sequence and charge state, the ion temperature obtained from C_n and C_n' tags was consistent for each peptide. Notably, when the b_S-ion temperature remained constant within ±5 K, the majority of the peptide fragment spectra represented by the y-ions was very reproducible even though the b-ion fragment patterns in the low-mass region significantly varied with the tag.

DISCUSSION

The canonical rate constant obtained from theory provides Arrhenius parameters E_a and A for $k(T) = A\exp(-E_a/RT)$. The activation energy E_a is approximately equal to $E_a = \Delta H^{\ddagger}_{0K} + 1.3RT$. Considering a difference in heat capacity between the transition state and the b_S ion, the activation energy can be expressed as $E_a = \Delta H^{\ddagger}_{700K} + 0.6RT$. Thus, it is mainly the variation in $\Delta H^{\ddagger}_{0K}$ that leads to a decrease in E_a for C_n tags and an increase in E_a for C_n' tags as the alkyl chain length n increases. The entropy of activation calculated from vibrational partition functions of the transition state and the b_S ion was in the range of 7.9−8.5 eu at 700 K. These values of $\Delta S^{\ddagger}_{700K}$ resulted in log A = 15.2−15.4 from the relationship in eq 7.[32]

$$A = \exp(1)\frac{k_B T}{h}\exp\left(\frac{\Delta S^{\ddagger}}{R}\right) \quad (7)$$

An average value of log A = 15.3 with $\Delta S^{\ddagger}_{700K}$ = 8.0 eu indicates a loose transition state for the CO-loss process, which is in line with the productlike transition state, as shown in Figure 4. Moreover, the disintegration of the transition state to the a_S ion plus CO always proceeds with a positive entropy change. Thus, the overall CO-loss process in the N-protonated oxazolone occurs without an entropic bottleneck. Consequently, the ion temperature can be determined from the thermometer ion by using statistical rate theory.

The key assumption made in our internal standard approach is that the b_S ion formed in a collision cell has a Boltzmann internal energy distribution. This is valid when the transit time is much longer than the time required for intramolecular vibrational-energy redistribution (IVR) of internal energy. The IVR is known to take place in picoseconds,[28] whereas the transit time is on the order of a few to tens of microseconds. Under the present experimental conditions, the transit time is sufficiently long for the b_S ion to reach a thermal equilibrium. If a small fraction of an internal energy of the peptide ion is dissipated into the fragment kinetic energy and the internal energy is statistically distributed among fragments, the b_S-ion temperature determined from the a_S-ion yield would be slightly less than or equal to the temperature of the peptide ion activated by collision. Thus, the b_S-ion temperature represents a lower limit of the temperature of the activated peptide ion. In the case of bradykinin, our result can be compared with the previous study. Williams and co-workers reported the effective ion temperatures of 476−591 K for several modified bradykinin ions collisionally activated by sustained off-resonance irradiation in the ICR cell with a reaction delay of 0.5 s.[11] This ion temperature is significantly lower than 654 ± 4 K obtained in this work for the b_S ion derived from double protonated C_n- or C_n'-tagged bradykinin excited by collision with argon for 60 μs in ESI-Q-TOF. This discrepancy is ascribed to the difference in

dx.doi.org/10.1021/jp308697v | J. Phys. Chem. B 2012, 116, 13982−13990

reaction time delay or transit time and sequence modification. Apparently, a short transit time causes a kinetic shift in appearance energy of the fragment ion, and the N-acylated dipeptide tag increases the internal degrees of freedom and heat capacity of the peptide ion, thereby raising the ion temperature.

Nonetheless, the present methodology of using an internal standard to measure the ion temperature is robust and useful because of the following reasons: (1) the b_S ion is derived from the C_n or C_n' tag attached at the N-termini of peptides; (2) the unimolecular dissociation of the b_S ion occurs at E_a = 29.6−32.4 kcal mol^{-1} in parallel with other peptide backbone cleavage occurring at E_a = 30−40 kcal mol^{-1};[33,34] (3) the b_S ion is a sole source of the a_S ion; (4) the a_S-ion yield is a function of the b_S-ion temperature, independent of other peptide backbone cleavage. Therefore, this internal standard method using predetermined kinetic parameters listed in Table 1 is applicable to the temperature measurement of various peptide ions generated by MALDI and ESI. Such a peptide/fragment ion temperature can be a good parameter to obtain reproducible peptide fragment spectra, as shown in Figure 7 and Figure S5. Furthermore, it can provide fundamental data on thermochemical kinetics of the peptide backbone cleavage and important clues on structural rearrangements of peptide ions.

In addition to MBIT, there are several isobaric tags available for the simultaneous identification and quantification of proteins, which include isobaric tags for relative and absolute quantitation (iTRAQ),[35,36] the tandem mass tag (TMT),[37,38] the cysteine-specific cleavable isobaric labeled affinity tag (CILAT),[39] and the Caltech isobaric tag (CIT).[40] The iTRAQ incorporates ^{13}C, ^{15}N, and ^{18}O isotopes in the *N*-methylpiperazine acetic acid ester group.[35,36] The TMT employs ^{13}C and ^{15}N isotopes in the dimethylpiperidine moiety.[37,38] The CILAT adopts ^{13}C, ^{15}N, and ^{2}H isotopes in the piperazine derivative.[39] The CIT contains $^{1}H/^{2}H$-isotopes in the N,N-alkylated alanine residue.[40] Of them, only MBIT based on N-acylated dipeptides affords the N-protonated oxazolone ion (b_S) that undergoes CO-loss to yield the protonated imine ion (a_S).[16,17] Other tags provide the reporter ions that do not contain the leaving group CO, which prevents them from being used as internal standards for the temperature measurement. In the cases of MBITs, the sum of a_S and b_S can be used as the quantitation signal,[17] while the ratio of a_S to a_S + b_S can be used as a measure of the b_S-ion temperature. Furthermore, MBITs allow the $(N + 1)$-plex quantification of proteins using N pairs of different C_n or C_n' tags. Thus, the present methodology extends the capability of MBITs from isobaric multi-2-plex quantitation tags[17] to internal standards for measuring b_S-ion temperatures.

CONCLUSIONS

N-Acylated dipeptide tags (C_n or C_n' tags) attached to the N-termini of model peptides yield b_S ions having N-protonated 2- or 4-alkyl-substituted oxazolone structures upon tandem mass spectrometric analysis. The unimolecular dissociation of the N-protonated oxazolone ion showed a novel structure−reactivity relationship in the formation of a_S ion with loss of CO, which varied with the position and chain length of alkyl group on the N-protonated oxazolone ion. The 4-alkyl-substituted oxazolone ion lost CO faster than the 2-alkyl-substituted one. As the alkyl chain length increased from C_1 to C_8, the a_S-ion yield became higher for the 4-alkyl-substituted oxazolone ion and lower for the 2-alkyl-substituted one. Ab initio calculations suggested that the 4-alkyl substitution decreased the activation energy by stabilizing the positive charge on both the transition state and a_S ion, whereas the 2-alkyl substitution increased the activation energy by stabilizing the positive charge on the protonated oxazolone ion. The canonical rate constants obtained from theoretical potential energy surfaces allowed comparison of the a_S-ion yield between theory and experiment, which enabled the bracketing of the b_S-ion temperature within ±5 K. When the b_S-ion temperature was constant, the y-ion fragment spectra that provided the peptide sequence were nearly identical, independent of the tag. Thus, the N-acylated dipeptide tags can be used as internal standards for the precise measurement of ion temperature in peptide fragmentation, and the reproducible peptide fragment spectra could be obtained by controlling the ion temperature.

ASSOCIATED CONTENT

Supporting Information

The full-scale peptide fragment spectra, relative abundances of y and a/b ions, total electronic energies and zero-point energies of the b_S and a_S ions as well as the transition state, and the b_S-ion temperature determined from singly and doubly protonated model peptides labeled with C_n or C_n' tags. This material is available free of charge via the Internet at http://pubs.acs.org.

AUTHOR INFORMATION

Corresponding Author

*Tel: (+82) 54 279 2123. Fax: (+82) 54 279 3399. E-mail: skshin@postech.ac.kr.

Notes

The authors declare no competing financial interest.

ACKNOWLEDGMENTS

J.S. acknowledges the postdoctoral support from the Brain Korea 21 program administered by the Ministry of Education, Science and Technology (MEST) of Korea. This work was supported by the Functional Proteomics Center grant (no. FPR08A1-040) and the National Research Foundation grant (no. 2009-0086218) funded by MEST.

REFERENCES

(1) Biemann, K.; Martin, S. A. *Mass Spectrom. Rev.* **1987**, *6*, 1−75.
(2) Dongré, A. R.; Jones, J. L.; Somogyi, Á.; Wysocki, V. H. *J. Am. Chem. Soc.* **1996**, *118*, 8365−8374.
(3) Aebersold, R.; Mann, M. *Nature* **2003**, *422*, 198−207.
(4) Hoffman, E.; Stroobant, V. *Mass Spectrometry: Principles and Applications*; John Wiley and Sons: Hoboken, NJ, 2007.
(5) Karas, M.; Hillenkamp, F. H. *Anal. Chem.* **1988**, *60*, 2299−2301.
(6) Fenn, J. B.; Mann, M.; Meng, C. K.; Wong, S. F.; Whitehouse, C. M. *Science* **1989**, *246*, 64−71.
(7) Thibault, P.; Alexander, A. J.; Boyd, R. K.; Tomer, K. B. *J. Am. Soc. Mass Spectrom.* **1993**, *4*, 845−854.
(8) Vachet, R. W.; Glish, G. L. *J. Am. Soc. Mass Spectrom.* **1996**, *7*, 1194−1202.
(9) Schnier, P. D.; Price, W. D.; Jockusch, R. A.; Williams, E. R. *J. Am. Chem. Soc.* **1996**, *118*, 7178−7189.
(10) Schnier, P. D.; Price, W. D.; Strittmatter, E. F.; Williams, E. R. *J. Am. Soc. Mass Spectrom.* **1997**, *8*, 771−780.
(11) Schnier, P. D.; Jurchen, J. C.; Williams, E. R. *J. Phys. Chem. B* **1999**, *103*, 737−745.
(12) Moon, J. H.; Yoon, S. H.; Kim., M. S. *J. Phys. Chem. B* **2009**, *113*, 2071−2076.
(13) Kenttamaa, H. I.; Cooks, R. G. *Int. J. Mass Spectrom. Ion Processes* **1985**, *64*, 79−83.

(14) Wysocki, V. H.; Kenttamaa, H. I.; Cooks, R. G. *Int. J. Mass Spectrom. Ion Processes* **1987**, *75*, 181−208.
(15) Boering, K. A.; Rolfe, J.; Brauman, J. I. *Rapid Commun. Mass Spectrom.* **1992**, *5*, 406−414.
(16) Seo, J.; Suh, M.-S.; Thangadurai., T. D.; Kim., J.; Rhee, Y. H.; Yoon, H.-J.; Shin, S. K. *Anal. Chem.* **2008**, *80*, 6145−6153.
(17) Suh, M.-S.; Seo, J.; Thangadurai, T. D.; Rhee, Y. H.; Shin, S. K.; Yoon, H.-J. *Analyst* **2011**, *136*, 1614−1619.
(18) Seo, J.; Yoon, H.-J.; Shin, S. K. *J. Am. Soc. Mass Spectrom.* **2011**, *22*, 1668−1677.
(19) Nold, M. J.; Wesdemiotis, C.; Yalcin, T.; Harrison, A. G. *Int. J. Mass Spectrom. Ion Processes* **1997**, *164*, 137−153.
(20) Paizs, B.; Lendvay, G.; Vékey, K.; Suhai, S. *Rapid Commun. Mass Spectrom.* **1999**, *13*, 525−533.
(21) Paizs, B.; Suhai, S. *Rapid Commun. Mass Spectrom.* **2001**, *15*, 2307−2323.
(22) Polfer, N. C.; Oomens, J.; Suhai, S.; Paizs, B. *J. Am. Chem. Soc.* **2005**, *127*, 17154−17155.
(23) Polfer, N. C.; Oomens, J.; Suhai, S.; Paizs, B. *J. Am. Chem. Soc.* **2007**, *129*, 5887−5897.
(24) Yoon, S. H.; Chamot-Rooke, J.; Perkins, B. R.; Hilderbrand, A. E.; Poutsma, J. C.; Wysocki, V. H. *J. Am. Chem. Soc.* **2008**, *130*, 17644−17645.
(25) Paizs, B.; Szlávik, Z.; Lendvay, G.; Vékey, K.; Suhai, S. *Rapid Commun. Mass Spectrom.* **2000**, *14*, 746−755.
(26) El Aribi, H.; Rodriquez, C. F.; Almeida, D. R. P.; Ling, Y.; Mak., W. W.-N.; Hopkinson, A. C.; Siu, K. W. M. *J. Am. Chem. Soc.* **2003**, *125*, 9229−9236.
(27) El Aribi, H.; Orlova, G.; Rodriquez, C. F.; Almeida, D. R. P.; Hopkinson, A. C.; Siu, K. W. M. *J. Phys. Chem. B* **2004**, *108*, 18743−18749.
(28) Baer, T.; Hase, W. L. *Unimolecular Reaction Dynamics: Theory and Experiments*; Oxford University Press: New York, 1996.
(29) Frisch, M. J.; Trucks, G. W.; Schlegel, H. B.; Scuseria, G. E.; Robb, M. A.; Cheeseman, J. R.; Montgomery, J. A., Jr.; Vreven, T.; Kudin, K. N.; Burant, J. C. et al. *Gaussian 03, Revision B.04*; Gaussian, Inc., Pittsburgh, PA, 2003.
(30) Peng, C.; Ayala, P. Y.; Schlegel, H. B.; Frisch, M. J. *J. Comput. Chem.* **1996**, *17*, 49−56.
(31) Scott, A. P.; Radom, L. *J. Phys. Chem.* **1996**, *100*, 16502−16513.
(32) Houston, P. L. *Chemical Kinetics and Reaction Dynamics*; Dover Publications, Inc.: Mineola, NY, 2006.
(33) Csonka, I. P.; Paizs, B.; Lendvay, G.; Suhai, S. *Rapid Commun. Mass Spectrom.* **2000**, *14*, 417−431.
(34) Zhang, Z. *Anal. Chem.* **2004**, *76*, 3908−3922.
(35) Ross, P. L.; Huang, Y. N.; Marchese, J. N.; Williamson, B.; Parker, K.; Hattan, S.; Khainovski, N.; Pillai, S.; Dey, S.; Daniels, S.; Purkayastha, S.; Juhasz, P.; Martin, S.; Barlet-Jones, M.; He, F.; Jacobson, A.; Pappin, D. J. *Mol. Cell. Proteomics* **2004**, *3*, 1154−1169.
(36) Choe, L.; D'Ascenzo, M.; Relkin, N. R.; Pappin, D.; Ross, P.; Williamson, B.; Guertin, S.; Pribil, P.; Lee, K. H. *Proteomics* **2007**, *7*, 3651−3660.
(37) Dayon, L.; Hainard, A.; Licker, V.; Turck, N.; Kuhn, K.; Hochstrasser, D. F.; Burkhard, P. R.; Sanchez, J.-C. *Anal. Chem.* **2008**, *80*, 2921−2931.
(38) Dayon, L.; Turck, N.; Kienle, S.; Schulz-Kanppe, P.; Hochstrasser, D. F.; Scherl, A.; Sanchez, J.-C. *Anal. Chem.* **2010**, *82*, 848−858.
(39) Zeng, D.; Li, S. *Bioorg. Med. Chem. Lett.* **2009**, *19*, 2059−2061.
(40) Sohn, C. H.; Lee, J. E.; Sweredoski, M. J.; Graham, R. L. J.; Smith, G. T.; Hess, S.; Czerwieniec, G.; Loo, J. A.; Deshaies, R. L.; Beauchamp, J. L. *J. Am. Chem. Soc.* **2012**, *134*, 2672−2680.